Chemical Science

ROYAL SOCIETY OF CHEMISTRY

EDGE ARTICLE

View Article Online
View Journal | View Issue

Cite this: *Chem. Sci.*, 2024, **15**, 2074

All publication charges for this article have been paid for by the Royal Society of Chemistry

Received 11th November 2023
Accepted 20th December 2023

DOI: 10.1039/d3sc06059d

rsc.li/chemical-science

Overall reaction mechanism of photocatalytic CO_2 reduction on a Re(I)-complex catalyst unit of a Ru(II)–Re(I) supramolecular photocatalyst†

Kei Kamogawa, [a] Yuki Kato,*[b] Yusuke Tamaki, ‡[a] Takumi Noguchi, [b] Koichi Nozaki, [c] Tatsuo Nakagawa[d] and Osamu Ishitani *[ae]

Rhenium(I) complexes *fac*-[Re^{I}(diimine)(CO)$_3$(L)]$^{n+}$ are mostly used and evaluated as photocatalysts and catalysts in both photochemical and electrochemical systems for CO_2 reduction. However, the selective reduction mechanism of CO_2 to CO is unclear, although numerous mechanistic studies have been reported. A Ru(II)–Re(I) supramolecular photocatalyst with *fac*-[Re^{I}(diimine)(CO)$_3${OC(O)OCH$_2$CH$_2$NR$_2$}] (R = C_2H_4OH) as a catalyst unit (**RuC2Re**) exhibits very high efficiency, selectivity, and durability of CO formation in photocatalytic CO_2 reduction reactions. In this work, the reaction mechanism of photocatalytic CO_2 reduction using **RuC2Re** is fully clarified. Time-resolved IR (TR-IR) measurements using rapid-scan FT-IR spectroscopy with laser flash photolysis verify the formation of **RuC2Re(COOH)** with a carboxylic acid unit, *i.e.*, *fac*-[Re^{I}(diimine)(CO)$_3$(COOH)], in the photocatalytic reaction solution. Additionally, this important intermediate is detected in an actual photocatalytic reaction using steady state irradiation. Kinetics analysis of the TR-IR spectra and DFT calculations demonstrated the reaction mechanism of the conversion of the one-electron reduced species of **RuC2Re** with a *fac*-[Re^{I}(diimine$^{\bullet-}$)(CO)$_3${OC(O)OCH$_2$CH$_2$NR$_2$}]$^-$ unit, which was produced *via* the photochemical reduction of **RuC2Re** by 1,3-dimethyl-2-phenyl-2,3-dihydro-1*H*-benzo[*d*]imidazole (BIH), to **RuC2Re(COOH)**. The kinetics of the recovery processes of the starting complex **RuC2Re** from **RuC2Re(COOH)** accompanying the release of CO and OH^- was also clarified. As a side reaction of **RuC2Re(COOH)**, a long-lived carboxylate–ester complex with a *fac*-[Re^{I}(diimine)(CO)$_3$(COOC$_2$H$_4$NR$_2$)] unit, which was produced by the nucleophilic attack of TEOA to one of the carbonyl ligands of **RuC2Re(CO)** with a *fac*-[Re^{I}(diimine)(CO)$_4$]$^+$ unit, was formed during the photocatalytic reaction. This complex works not only as a precursor in another minor CO formation process but also as an external photosensitiser that photochemically reduces the other complexes *i.e.*, **RuC2Re**, **RuC2Re(COOH)**, and the intermediate that is reductively converted to **RuC2Re(COOH)**.

Introduction

Photocatalytic CO_2 reduction using visible light as an energy source has the potential to solve three serious problems for humankind, *i.e.*, global warming and the shortage of both energy and carbon resources.[1,2] In particular, the two-electron reduction from CO_2 to CO, that can proceed at relatively low overpotentials *via* proton coupled two-electron reduction (eqn (1) at pH 7) or reductive disproportionation (eqn (2)), has attracted attention because CO is a useful intermediate for the synthesis of high-energy and useful carbon materials.

$$CO_2 + 2H^+ + 2e^- \rightarrow CO + H_2O,\ E^\circ = -0.53\ \text{V}\ \textit{vs.}\ \text{NHE} \quad (1)$$

$$2CO_2 + 2e^- \rightarrow CO + CO_3^{2-},\ E^\circ = -0.64\ \text{V}\ \textit{vs.}\ \text{NHE} \quad (2)$$

In 1983, *fac*-[Re(bpy)(CO)$_3$X] (bpy = 2,2′-bipyridine, X = Cl or Br) was first reported by Lehn *et al.* as an efficient CO_2 reduction photocatalyst. This photocatalytic reaction proceeded in a mixed solution of *N*,*N*′-dimethylformamide (DMF) and triethanolamine (TEOA) (5 : 1 v/v) with the very high selectivity of CO as a reduction product without the formation of H_2 even in the presence of water and without the formation of formic acid.

[a]*Department of Chemistry, School of Science, Tokyo Institute of Technology, 2-12-1-NE-2 O-okayama, Meguro-ku, Tokyo 152-8550, Japan. E-mail: ishitani@chem.titech.ac.jp*

[b]*Department of Physics, Graduate School of Science, Nagoya University, Nagoya 464-8602, Japan. E-mail: yuki.kato@bio.phys.nagoya-u.ac.jp*

[c]*Department of Chemistry, Graduated School of Science and Engineering, University of Toyama, 3190, Gofuku, Toya-ma-shi, Toyama 930-8555, Japan*

[d]*UNISOKU Co., Ltd, 2-4-3 Kasugano, Hirakata, Osaka, 573-0131, Japan*

[e]*Department of Chemistry, Graduate School of Advanced Science and Engineering, Hiroshima University, 1-3-1 Kagamiyama, Higashi-Hiroshima, Hiroshima 739 8526, Japan*

† Electronic supplementary information (ESI) available. See DOI: https://doi.org/10.1039/d3sc06059d

‡ Present Address: National Institute of Advanced Industrial Science and Technology (AIST), 4-2-1 Nigatake, Miyaginoku, Sendai, Miyagi 983-8551, Japan.

After this report, many transition-metal-complex catalysts such as Re(I),[3–7] Ru(II),[8,9] Fe(II),[10–13] Co(I),[10,14–18] Ni(I)[19–21] and Mn(I)[22,23] complexes were reported for the photocatalytic reduction of CO_2 to CO. Although mechanistic studies on these photocatalytic reactions have been continuously reported, mechanistic insights into the photocatalytic reactions, such as the structures of the intermediates and reaction rates of each process during the photocatalytic CO_2 reduction, have been insufficient for the systematic design of better photocatalysts and the addition of new functions to the photocatalysts.

A typical example is the mechanism of photocatalytic CO_2 reduction using *fac*-[Re(diimine)$(CO)_3$X] as the photocatalyst. Many researchers have been interested in the selective formation mechanism of CO in photocatalytic CO_2 reduction as well as the electrocatalytic reduction of CO_2 using the Re complexes as catalysts.[3–7,24] Kubiak *et al.* used the stopped-flow method with a rapid scan FT-IR detector in the reaction of a five-coordinated 18e$^-$ species [Re(4,4′-di-*tert*-butyl-bpy)$(CO)_3]^-$ with CO_2 and detected a carboxylic acid complex.[25] In many systems using metal-complex photocatalysts that reduce CO_2 to CO, the corresponding carboxylic acid complexes have been assumed to be intermediates based on the mechanistic studies on chemical and/or electrocatalytic CO_2 reduction.[1,25–40] However, the mechanism of the photocatalytic reaction was too potentially different to be clarified based on only the mechanisms of the chemical and electrochemical CO_2 reduction reactions even when using the same catalyst; this is because the initial step of the photocatalytic reactions was a one-electron reduction of the catalyst but not a two-electron reduction. In other words, the one-electron reduced catalyst has an adequate lifetime for changing its structure, *i.e.*, the formation of another intermediate or other intermediates before accepting the second electron from another molecule with sufficient reduction power to reduce the intermediate(s) that proceeds *via* diffusion collision. This second electron injection process to the intermediate(s) made from the one-electron reduced catalysts is considerably slower compared to those in the electrocatalytic CO_2 reduction reactions in which the electrode can simultaneously supply electrons.[1]

In the reaction mechanism of the "photocatalytic" CO_2 reduction using the Re catalysts, Inoue *et al.* identified an "oxidized" carboxylic acid complex [Re^{II}(dmb)$(CO)_3$(COOH)]$^+$ (dmb = 4,4′-dimethyl-2,2′-bipyridyl) in the photocatalytic reaction of *fac*-[Re(dmb)$(CO)_3$Cl] using triethylamine (TEA) as a sacrificial electron donor in a DMF solution using cold-spray ionization spectroscopy and operando measurements using XAFS and FT-IR.[27,28] Fujita *et al.* identified a di-nuclear Re complex with a carboxylate bridging ligand when the penta-coordinated 17e$^-$ species [Re(dmb)$(CO)_3]^0$ was produced *via* the photocleavage of the Re–Re bond of [Re(dmb)$(CO)_3]_2$ in CO_2 saturated dry DMF.[41,42]

Notably, in most reported efficient photocatalytic reactions using the Re-complex catalyst and/or photocatalyst including Lehn's system, DMF or *N*,*N*′-dimethylacetamide (DMA) containing a high concentration of TEOA, typically DMF : TEOA = 5 : 1, the use of these solutions can enhance the durability, efficiency, and selectivity of the photocatalytic CO_2 reduction to CO compared with those using other solvents and additives such as MeCN and TEA.[3–6,43] We previously demonstrated that one of the advantages of the high concentration of TEOA is that TEOA assists CO_2 capture into the Re(I) complex (eqn (3)).[5] In the photocatalytic reaction by *fac*-[Re(bpy)$(CO)_3$Br] in the DMF–TEOA (5 : 1 v/v) mixed solution, *i.e.*, same as Lehn's system, it was elucidated that in the initial stage of the photocatalytic reaction, *fac*-[Re(bpy)$(CO)_3$Br] is rapidly converted to the corresponding carbonate ester complex, *i.e.*, *fac*-[Re(bpy)$(CO)_3${OC(O)$OCH_2CH_2NR_2$}] (R = C_2H_4OH) that acts as a catalyst for CO_2 reduction, and the residual *fac*-Re(bpy)$(CO)_3$Br acts as a redox photosensitiser that initiates photochemical one-electron transfer from TEOA to *fac*-[Re(bpy)$(CO)_3${OC(O)$OCH_2CH_2NR_2$}]. In many photocatalytic systems using Re(I) complexes as a "photocatalyst" in the presence of TEOA, similar reactions are expected, *i.e.*, these photocatalytic systems work as two-component systems including the carbonate ester Re(I) complex as a catalyst and the starting emissive Re(I) complex, with an excited state that can be reductively quenched by TEOA, as a photosensitiser. The addition of [Ru(diimine)$_3]^{2+}$ as an additional photosensitiser and a suitable reductant drastically enhances the photocatalysis of the system including the Re(I) complex and TEOA.[44,45]

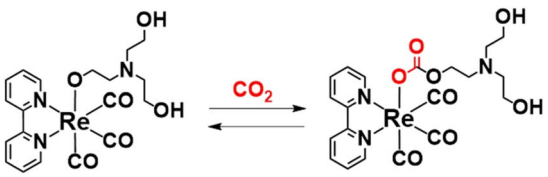

(3)

Supramolecular photocatalysts, in which the [Ru(diimine)$_3]^{2+}$ redox photosensitiser and Re(I) catalyst units are connected by an ethylene chain, promote higher photocatalytic activity compared with a mixed system involving corresponding mononuclear Ru(II) and Re(I) complexes owing to rapid intramolecular electron transfer from the photosensitiser to the catalyst unit.[45] From a mechanistic viewpoint, supramolecular photocatalysts are useful because the rapid electron transfer process from the reduced photosensitiser to the catalyst can be kinetically separated from CO_2 reduction processes on the reduced Re unit, which are much slower compared to the intramolecular electron transfer. In these systems, we can omit the direct photoexcitation of the Re complexes using long-wavelength light (typically 480 nm), which only the Ru photosensitiser unit can absorb.

In the photocatalytic system using a supramolecular photocatalyst consisting of the Ru(II) photosensitiser and *fac*-[Re(diimine)$(CO)_3${OC(O)$OC_2H_4NR_2$}] catalyst units (**RuC2Re**), kinetic studies on the formation processes of the one-electron reduced species (OERS) of the Re unit, which is one of the key intermediates in the initial stage of photocatalytic CO_2 reduction, and its reactivity, were clarified using time-resolved IR (TR-IR) measurements using the pump–probe method and TR-vis measurements using the Randomly Interleaved Pulse Train (RIPT) method (Scheme 1).[46,47] These results clearly indicated that the OERS of **RuC2Re** is produced by two processes: (1) a fast

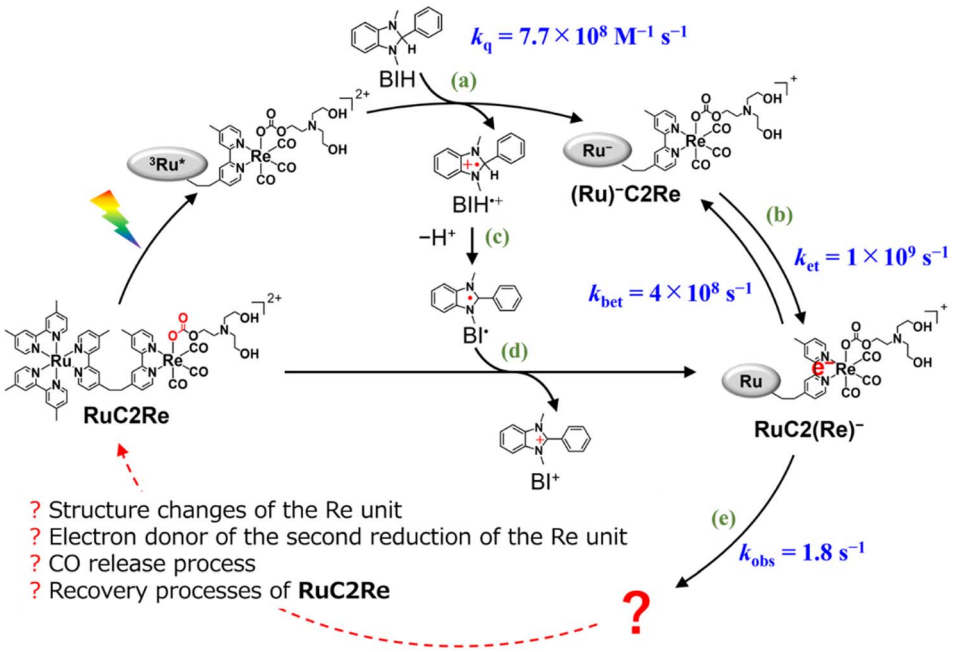

Scheme 1 Formation processes of the one-electron reduced species (OERS) of **RuC2Re** and unknown processes shown as "?".

process lasting several tens of nanoseconds after excitation, which is reductive quenching of the excited state of the Ru unit to yield the OERS of the Ru unit, *i.e.*, **(Ru)$^-$C2Re** (Scheme 1, Process (a)), followed by fast intramolecular electron transfer to the Re unit to produce another OERS, *i.e.*, **RuC2(Re)$^-$** in which the Re unit accepts one electron (Process (b)); and (2) a slower process lasting several tens of microseconds, which is attributed to the reduction of **RuC2Re** in the ground state by BI$^\bullet$ (Process (d)), which is produced by the deprotonation of BIH$^{\bullet+}$ (Process (c)).

The intramolecular electron transfer from the reduced Ru unit to the Re unit, with a rate constant ($k_{et} = 1 \times 10^9$ s^{-1}, $k_{bet} = 4 \times 10^8$ s^{-1}) that was determined in this study, was a much faster process compared to the following processes; the two intermediates **(Ru)$^-$C2Re** and **RuC2(Re)$^-$** could be spectroscopically observed. After the intramolecular electron transfer, the subsequent reaction of the **RuC2(Re)$^-$** (Process (e)) proceeded at a relatively slow rate ($k_{obs} = 1.8 \pm 0.1$ s^{-1} at 298 K). The intermediates produced after this slow reaction could not be observed because it was difficult to prevent the diffusion of transient species in the solution during the measurements using the pump–probe and RIPT methods.[48–51]

In this work, we successfully clarified the unknown subsequent reaction mechanism after the intramolecular electron transfer in the photocatalytic CO_2 reduction on the Re catalyst unit, which is shown as "?" in Scheme 1, by applying various methods, *i.e.*, TR-IR spectroscopy using the rapid scan FT-IR method, which is more suitable for tracking the reaction that proceeds on the time scale from milliseconds to minutes, liquid chromatography analysis of the photocatalytic reaction solutions, and DFT calculations. This is the first report on the whole picture of the CO_2 reduction mechanism on the Re catalyst in the photocatalytic systems.

Results

Rapid-scan time-resolved FT-IR measurements coupled with laser flash photolysis

A CO_2 saturated DMSO–TEOA (5 : 1 v/v) mixed solution containing **RuC2Re** (1.0 mM) and BIH (0.1 M) as a sacrificial electron donor in an optical cell was irradiated with the second harmonic of a pulsed Nd : YAG laser (532 nm) once every 10 min. Notably, under these reaction conditions using an LED continuous light source at $\lambda_{max} = 530$ nm instead of laser pulses, **RuC2Re** can reduce CO_2 to CO with high TON (>2000), quantum yield (=40%), and selectivity (>99%), which is similar to the photocatalysis of **RuC2Re** measured in the DMA–TEOA (5 : 1 v/v) mixed solution.[46,52] Because the photocatalyst was finally recovered to the original structure within the pulse interval (10 min) described below, the solution did not flow during the measurements. In addition, because of the large diameter of the excitation pulse (~1 cm), the diffusion of the transient species was not a problem for the measurements. **RuC2Re** shows vibrational absorption bands of the CO ligands at 2018, 1911, and 1888 cm^{-1}, the C=O moiety of the carbonate ester ligand at 1668 cm^{-1} and both the dmb ligands of the Ru and Re units at 1619 cm^{-1} (Fig. S1†).[46]

Fig. 1a shows the TR-IR spectra from 21 ms to 3.0 s after the laser flash illumination. At 21 ms, there was an appearance of bleaching bands at 2019, 1911, 1894 (sh), 1672, and 1620 cm^{-1} (marked with black stars in Fig. 1a), which originated from the consumption of **RuC2Re**, and new absorption bands at 1994, 1876 (sh), 1859, 1639, 1590 and 1575 cm^{-1} (marked with red circles), which were attributed to the OERS of the Re unit **RuC2(Re)$^-$**.[46,53–55] These spectral changes are identical to the previously reported TR-IR spectra measured by the pump–probe method at several ns to ms after laser irradiation.[46] These

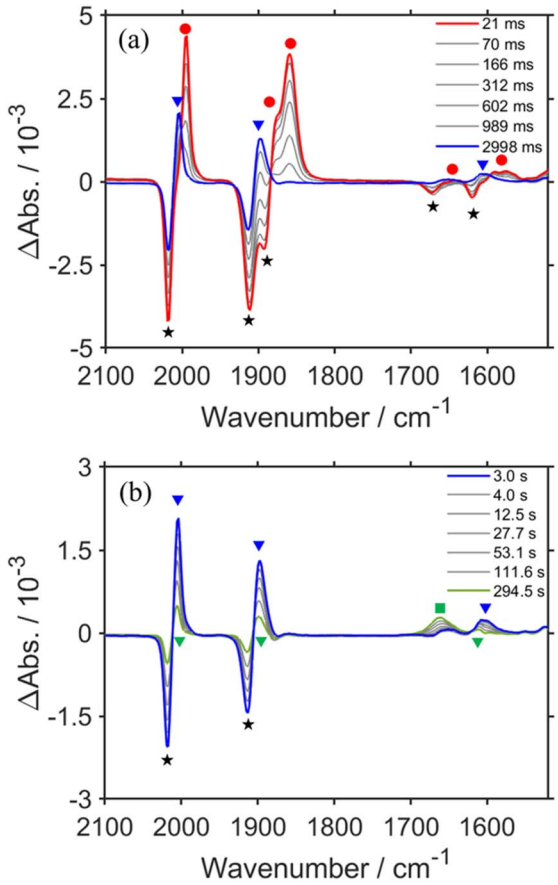

Fig. 1 TR-IR spectra of CO_2 saturated DMSO–TEOA (5 : 1 v/v) solution containing **RuC2Re** (1.0 mM) and BIH (0.1 M) (a) from 21 ms to 3.0 s and (b) from 3.0 s to 5.0 min after pulsed excitation at 532 nm. A total of 50 loops of spectra using the two samples were averaged for the final data.

results clearly indicate that we could successfully apply the rapid-scan time-resolved FT-IR measurements with the laser flash photolysis to the photochemical formation of **RuC2(Re)**$^-$, which is produced by electron transfer from BIH to the excited Ru unit, and intramolecular electron transfer from the reduced Ru unit to the Re unit as well as the reduction of **RuC2Re** by BI$^\bullet$ as described in the Introduction section (Scheme 1).

DFT calculations (Table S1†) were performed to obtain the ν_{CO} values of a model mononuclear complex of the Re catalyst unit of **RuC2Re** and **RuC2(Re)**$^-$, *i.e.*, *fac*-[Re(dmb)(CO)$_3${OC(O)OC$_2$H$_4$NR$_2$}] (R = CH_2CH_2OH, dmb = 4,4′-dimethyl-2,2′-bipyridine) (**Re**) and its OERS (**Re**$^-$). It should be noted that the electronic interactions between the Ru and Re units, which are connected by the ethylene chain in **RuC2Re** and its derivatives, are weak.[46,56,57] The results are presented in Table S1,† in which the calculated and experimental ν_{CO} values are in good agreement. Therefore, we used the DFT calculation as one of the methods for investigating the short-lived intermediates as described below.

From 21 ms after the laser flash, the positive bands of **RuC2(Re)**$^-$ slowly decayed and new peaks were clearly observed at 2004, 1898, and 1606 cm^{-1} (marked with blue triangles in Fig. 1a) with isosbestic points at 2001, 1884, and 1595 cm^{-1}. These changes were completed until 3.0 s after the laser flash. During this period, the bleaching bands decayed to approximately half of their intensity. The newly appeared peaks were very similar to those of a mononuclear carboxylic acid complex *fac*-[Re^{I}(dmb)(CO)$_3$(COOH)] (Fig. S2†), which showed ν_{CO}s at 2004 and 1893 cm^{-1}; two other peaks were observed at 1620 and 1606 cm^{-1} as well. The product in this time scale is attributable to a carboxylic acid complex **RuC2Re(COOH)**, of which the Re unit has a *fac*-[Re^{I}(diimine)(CO)$_3$(COOH)] structure (Scheme 2). Because the calculated vibrational energy of the stretching band of the C=O group in the carboxylic acid ligand of *fac*-[Re^{I}(dmb)(CO)$_3$(COOH)] was smaller than that of the dmb ligand (Table S1†), the peaks at 1620 and 1606 cm^{-1} in the IR of *fac*-[Re^{I}(dmb)(CO)$_3$(COOH)] were attributed to the stretching bands of the dmb ligand and the C=O group of the carboxylic acid ligand, respectively. The peak attributable to the dmb stretching vibration of the Re unit of **RuC2Re(COOH)** was not clearly identified in the TR-IR spectra likely because the energy of this vibration is very similar to those of both the Ru and Re units of **RuC2Re**. These peak assignments are summarized in Table 1.

To confirm the peak assignments described above, the same experiments were performed under a $^{13}CO_2$ atmosphere. The broad negative band at ν_{max} = 1672 cm^{-1}, which was observed under an ordinary CO_2 atmosphere, was not observed at the TR-IR spectrum measured immediately after the laser flash, and another negative peak was observed as a shoulder at ~1640 cm^{-1} (Fig. 2a and S3a†). This strongly supports that these negative bands, *i.e.*, ν_{max} = 1672 cm^{-1} under ordinary CO_2 and $\nu_{shoulder}$ ~ 1640 cm^{-1} under $^{13}CO_2$, were attributed to the C=O stretching of the carbonyl ester ligand of **RuC2Re**. The weak positive band at ν_{max} = 1639 cm^{-1} observed under ordinary CO_2, which is attributed to the C=O vibrational band of **RuC2(Re)**$^-$, was not observed under $^{13}CO_2$ and a replacement peak was not clearly observed as well. This is reasonable because the band under $^{13}CO_2$ was shifted to a lower frequency and was overlapped by the stronger negative peak of the dmb ligand at ν_{max} = 1620 cm^{-1}, which was observed both under ordinary CO_2 and under $^{13}CO_2$. The bands attributed to the CO ligands (bleaching bands at 2019, 1911 and 1894 (sh) cm^{-1}; positive bands at 1994, 1876 (sh), and 1859 cm^{-1}) did not change. At 3.0 s after laser irradiation (Fig. 2b and S3b†), the positive peak attributable to the C=O vibrational band of the

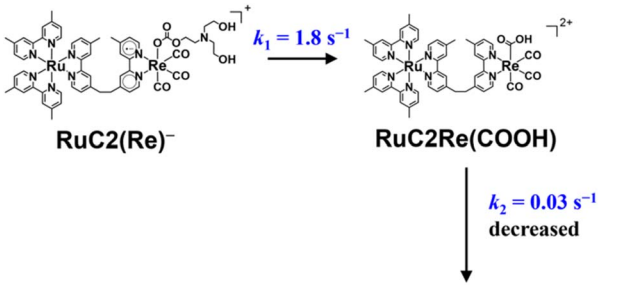

Scheme 2 Conversion reaction from **RuC2(Re)**$^-$ to **RuC2Re(COOH)** and the rate constant of the following process.

Table 1 Vibrational bands observed in TR-IR measurements and their assignments

Complex	IR absorption/cm^{-1}
RuC2Re (★)	2019, 1911, 1894 (sh) [CO ligands] 1672 [C=O of the carbonate ester ligand] 1620 [dmb ligand]
RuC2(Re)$^-$ (●)	1994, 1876 (sh), 1859 [CO ligand] 1639 [C=O of the carbonate ester ligand] 1590, 1575 [dmb ligand]
RuC2Re(COOH) (▼)	2004, 1898 [CO ligands] 1606 [C=O of the carboxylic acid ligand]
RuC2Re(CO-TEOA) (▼)	2006, 1900 [CO ligands] 1611 [C=O of the carboxylate ester ligand]
HCO$_3^-$ (■)	1662

carboxyl ligand of **RuC2Re(COOH)** observed at 1606 cm^{-1} under ordinary CO_2 was shifted to the 38 cm^{-1} lower wavenumber under $^{13}CO_2$, *i.e.*, ν_{max} = 1568 cm^{-1} (although small shoulder peaks were also observed at 1992 and 1859 cm^{-1} as shown in Fig. S3b,† these should be attributed to the ^{13}CO ligand(s) formed during the TR-IR measurements).[58] This lower shift of the C=O vibration of the carboxylic acid ligand is consistent with previous reports on [Re^{II}(dmb)(CO)$_3$(COOH)]$^+$ (−39 cm^{-1}) and the iron porphyrin carboxylic acid complex (−48 cm^{-1}).[28,36] It was also supported by the vibrational frequency predictions using the DFT calculation (−37 cm^{-1}; Table S1†). These results demonstrate that the carbonate ester ligand of **RuC2Re** originated from CO_2 and was converted to the carboxylic acid ligand during the photocatalytic reaction. In addition, similar experiments using TEOA with deuterated hydroxy groups and deuterated BIH at the second position of the dihydroimidazole ring were conducted with ordinary CO_2. The peak attributable to the C=O stretching of the carbonyl ester ligand of **RuC2Re(-COOH)** shifted to the 13 cm^{-1} lower wavenumber (Fig. S4†). This lower shift also supports the identification of the C=O stretching band because the DFT calculation of the complex with the *fac*-[Re^{I}(diimine)(CO)$_3$(COOD)] structure indicates that deuteration induces a lower shift of the C=O stretching band by −9 cm^{-1} compared to that with *fac*-[Re^{I}(diimine)(CO)$_3$(COOH)].

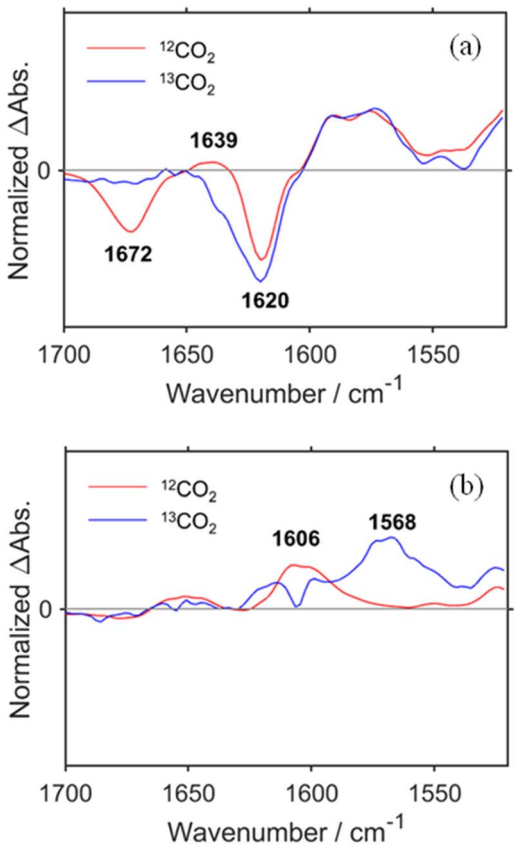

Fig. 2 TR-IR spectra measured in ordinary CO_2 (red) and $^{13}CO_2$ (blue) saturated DMSO–TEOA (5 : 1 v/v) solution containing **RuC2Re** (1.0 mM) and BIH (0.1 M) at (a) 21 ms and (b) 3.0 s after the laser flash. These spectra were normalized by absorbance at 2019 cm^{-1} at 21 ms after pulsed excitation.

The TR-IR spectra from 21 ms to 4.0 s after the laser flash were analyzed using a global sequential routine.[59,60] A good fitting was achieved by analysis using double components (Fig. S5†). The obtained evolution associated spectra (EAS) indicated that the first and second components were assigned to **RuC2(Re)**$^-$ and **RuC2Re(COOH)**, respectively. The rate constants were determined to be k_1 = 1.8 ± 0.1 s^{-1} and k_2 = 0.031 ± 0.008 s^{-1} (Scheme 2); the experimental errors were calculated using data from three independent experiments. Because k_1 is very close to the previously reported rate constant (1.8 ± 0.1 s^{-1}) of the subsequent reaction of **RuC2(Re)**$^-$, which was measured using UV-vis absorption spectroscopy,[46] the rate constants are assigned to the conversion reaction from **RuC2(Re)**$^-$ to **RuC2Re(COOH)** and the slower subsequent reaction of **RuC2Re(COOH)** (Scheme 2), which is discussed in details below. Notably, as previously reported, the faster spectral change could be fitted with a single exponential function, *i.e.*, its reaction rate linearly depends on the concentration of the OERS of **RuC2Re**.

Fig. 1b shows the TR-IR spectra from 3.0 s to 5 min after the laser flash. The positive peak assigned to **RuC2Re(COOH)** decayed. Although the recovery of the bleaching bands assigned to the starting complex **RuC2Re** was observed, it did not fully recover (approximately 90% recovery after 5 min) as described in detail below. In addition, a new peak was observed at 1662 cm^{-1} (marked with a green square in Fig. 1b), which is attributable to HCO$_3^-$ (Table 1): this identification was also supported by the fact that this peak shifted to the 44 cm^{-1} lower wavenumber in the same experiments under the $^{13}CO_2$ atmosphere (Fig. S3c and d†), which is consistent with the reported shift of HCO$_3^-$.[61] We reported that the amount of HCO$_3^-$ produced was similar to that of CO during the photocatalytic CO_2 reduction reaction using **RuC2Re** and BIH, and the overall reaction equation of the photocatalytic reaction is presented in eqn (4).[46]

$$2CO_2 + BIH \rightarrow CO + HCO_3^- + BI^+ \quad (4)$$

In the TR-IR measurements under the $^{13}CO_2$ atmosphere, the bleaching and positive bands assigned to **RuC2Re(COOH)** decayed and, in addition, another peak appeared at 1862 cm^{-1}, which is attributed to the ^{13}CO ligand increased during 5 min after the irradiation (Fig. S3c†). This result indicates that the ^{12}CO ligand attached on the central Re was sometimes released and the ^{13}CO ligand can remain in the Re complex during the TR-IR measurements. It has been reported that, in other photocatalytic reactions using similar Re(I) complexes as catalysts under a $^{13}CO_2$ atmosphere, the ^{12}CO ligands were gradually substituted with ^{13}CO.[27,58]

Because ~90% of the OERS of **RuC2Re** recovered to the non-reduced **RuC2Re** at 5 min after the irradiation (Fig. 1b), most of the CO formation from **RuC2Re(COOH)** proceeded during this period of time in the TR-IR measurement. This suggests that the CO formation from **RuC2Re(COOH)** is the rate-determining step or one of the rate-determining steps in the TR-IR measurement. It was reported that the photocatalytic CO_2 reduction proceeded with almost the same CO production rate (turnover frequency) when the photocatalytic reactions using a Ru(II)–Re(I) supramolecular photocatalyst were conducted between under pure CO_2 and under Ar containing 10% CO_2 atmospheres, *i.e.*, the photocatalytic reaction rate does not depend on the CO_2 concentration under these reaction conditions. These results suggest that **RuC2Re(COOH)** released CO and OH^-, and the released OH^- reacted with another CO_2 to form HCO_3^-.

The positive peaks of **RuC2Re(COOH)** observed at 3 s after the laser flash were upshifted slightly but clearly to 2006, 1900, and 1611 cm^{-1} without shifts of the bleaching band (Fig. 1b and S6†); these blue-shifted peaks remained even at 5 min after the laser flash as described above. The TR-IR spectral change between 2100 and 1700 cm^{-1} up to 5 min after the laser flash could be globally fitted with three components (Fig. 3): the low wavenumber region (1550–1700 cm^{-1}) was excluded because of the effect of the accumulated HCO_3^-. The first (EAS1; $k_1 = 1.8 \pm 0.1\ s^{-1}$) and second (EAS2; $k_2' = (4 \pm 1) \times 10^{-2}\ s^{-1}$) were similar to the results of the aforementioned global analysis of all the TR-IR spectra up to 4 s (Fig. S5†). The third component (EAS3) is long-lived ($k_3 = (3.0 \pm 0.6) \times 10^{-3}\ s^{-1}$) and has a slightly higher ν_{CO} (2006, 1900 cm^{-1}) compared to EAS2 which is attributed to **RuC2Re(COOH)**, which was consistent with the TR-IR spectrum at 5 min after excitation. This species is attributable to a carboxylate–ester complex **RuC2Re(CO-TEOA)** with the $[Re^I(diimine)(CO)_3\{C(O)OC_2H_4N(C_2H_4OH)_2\}]$ unit (eqn (5)). The identification of this additional intermediate is described in detail below. These results indicated that a part of the photochemically produced **RuC2Re(COOH)** did not return directly to **RuC2Re** but was converted to another long-lived complex **RuC2Re(CO-TEOA)**. Because the bleach of the band intensity of EAS3 was approximately 60% of that of EAS2, approximately 60% of the produced **RuC2Re(COOH)** was converted to **RuC2Re(CO-TEOA)** in the TR-IR measurement. $k_2'(k_2)$ is a rate constant that considers both the reaction of **RuC2Re(COOH)** directly back to **RuC2Re** and the conversion to the third component (**RuC2Re(CO-TEOA)**).

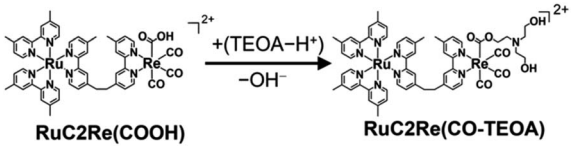

(5)

Notably, during the TR-IR measurements described in this section, **RuC2Re** was stable. Fig. S7† shows the FT-IR spectra of the reaction solution measured after every 10 laser irradiations (*e.g.*, the red and purple lines are the FT-IR spectra after the irradiation of pulses 10 and 60 times, respectively). The HCO_3^- (1662 cm^{-1}; Fig. S7a†) and free CO (2130 cm^{-1}; Fig. S7b†) clearly increased by the laser irradiation; however, only a very small amount (<5% based on **RuC2Re** used) of **RuC2Re(CO-TEOA)** (2006, 1900 cm^{-1}) was accumulated even after 60 laser pulses. Thus, neither the decomposition of complexes nor the accumulation of intermediates affected the measurement, *i.e.*, almost all of photoexcited complexes returned to the starting complex **RuC2Re** within the pulse interval in the TR-IR measurements (10 min).

FT-IR measurements during and after steady-state light irradiation

We measured the FT-IR spectra of a CO_2 saturated DMSO–TEOA (5 : 1 v/v) solution containing **RuC2Re** (2.0 mM) and BIH (0.1 M)

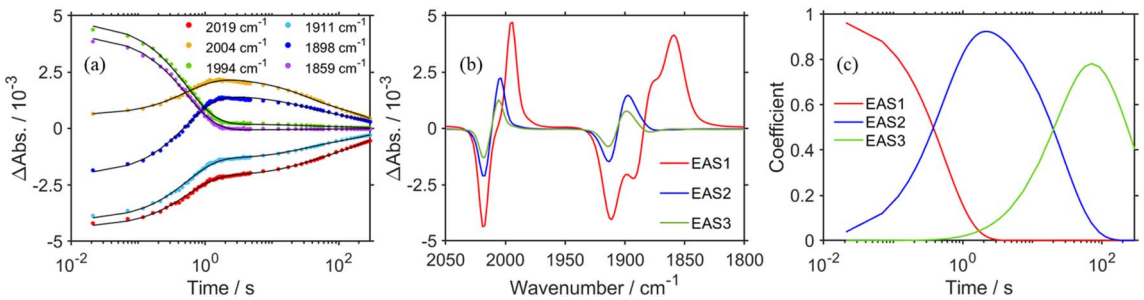

Fig. 3 (a) Kinetics traces (dots) of TR-IR spectra from 21 ms to 5.0 min at characteristic wavelengths with their fits obtained by global analysis using a three component global sequential fitting routine (black line). (b) Evolution-associated spectra (EAS) generated by global analysis of TR-IR spectra from 21 ms to 5 min after laser flash using three components. (c) Time-courses of EAS.

during steady-state light irradiation at 480 nm (Fig. 4a). The peaks at 2018, 1911, and 1888 cm^{-1} derived from **RuC2Re** decayed and the new peaks at 2004 and 1898 cm^{-1} appeared with isosbestic points at 2012 and 1906 cm^{-1}. Because the difference spectrum between the FT-IR spectra before and during irradiation (Fig. 4b) was quite similar to the TR-IR spectrum at 3.0 s after the laser flash (Fig. 1b), the peaks that appeared were mainly attributed to **RuC2Re(COOH)**. The concentration change of **RuC2Re** and **RuC2Re(COOH)** during the steady-state light irradiation (Fig. 4) was evaluated from the ν_{CO} peak derived from symmetry stretching vibration areas corresponding to each of the complexes; the peaks could be separated by curve fitting using a linear combination of the Gaussian function and Lorentzian functions (Fig. S8†). After ~100 s of irradiation, the concentrations of **RuC2Re** and **RuC2Re(COOH)** reached a photo-stationary state with the ratio of **RuC2Re** to **RuC2Re(COOH)** ≈ 1 : 2, *i.e.*, both production and consumption rates of **RuC2Re(COOH)** became equal during the irradiation (Fig. 4c). After the irradiation, the peaks of **RuC2Re(COOH)** decayed and those of **RuC2Re** recovered (Fig. 4d). This spectral change could be fitted with a single exponential function, and the rate constant was 0.025 s^{-1} after the solution was irradiated for 120 s and then irradiation was stopped (Fig. S9†). This value is close to $k_2' = (4 \pm 1) \times 10^{-2}$ s^{-1} (and $k_2 = (3.1 \pm 0.8) \times 10^{-2}$ s^{-1}) obtained by the TR-IR measurements, which is the rate constant of the subsequent reaction of **RuC2Re(COOH)** (Fig. 3 and S5†). These results clearly indicate that **RuC2Re(COOH)** is formed as the intermediate in the photocatalytic reaction of CO_2 reduction using a steady-state light source. Although the long-lived component **RuC2Re(CO-TEOA)** observed in the TR-IR measurements was not clearly observed in the steady-state irradiation owing to the low SN ratio, the shoulder peak at approximately 2005 cm^{-1} remained even at 183 s after the light irradiation stopped (Fig. 4d). Furthermore, the decay rate slowed with the increasing period of light irradiation (k = 0.027 s^{-1} (1 min), 0.025 s^{-1} (2 min), 0.023 s^{-1} (4 min)) (Fig. S9†). This indicates that the long-lived component accumulates with an increase in the light irradiation period. These results suggest that **RuC2Re(CO-TEOA)**, which is longer-lived than **RuC2Re(COOH)**, gradually accumulated during the steady-state light irradiation.

UHPLC analysis of photocatalytic reaction solutions

To clarify the structure of the long-lived intermediate during the steady-state irradiation, the photocatalytic reaction solutions were analyzed using ultra-high-performance liquid chromatography (UHPLC). Fig. 5a shows the chromatograms of the photocatalytic reaction solutions containing **RuC2Re** (0.5 mM) and BIH (0.1 M) before and after irradiation at λ_{ex} = 490–620 nm under a CO_2 atmosphere. The broad peak observed at 6–10 min

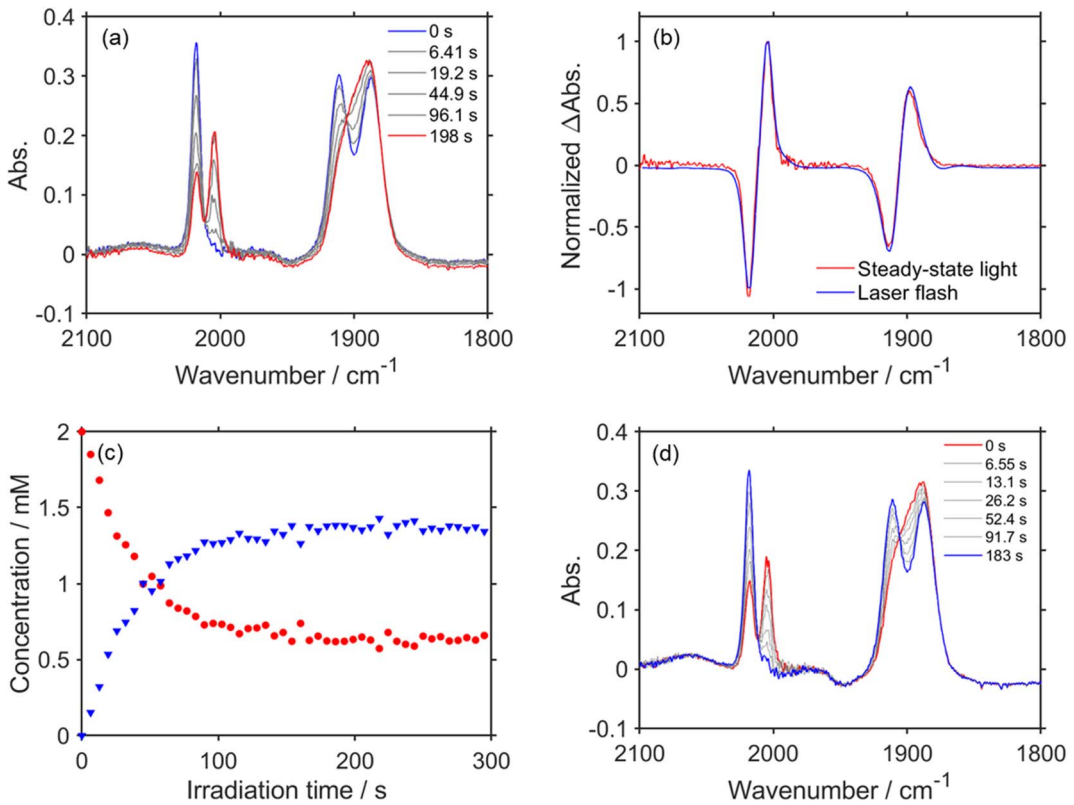

Fig. 4 (a) FT-IR spectra of CO_2 saturated DMSO–TEOA (5 : 1 v/v) solution containing **RuC2Re** (2.0 mM) and BIH (0.1 M) during steady-state light at 480 nm; d = 0.5 mm. (b) Normalized TR-IR spectrum at 3.0 s after laser flash (blue) and FT-IR spectrum after steady-state light irradiation for 198 s (red). (c) Concentration changes of **RuC2Re** (red) and **RuC2Re(COOH)** (blue) during steady-state light irradiation. (d) FT-IR spectra of CO_2 saturated DMSO–TEOA (5 : 1 v/v) solution containing **RuC2Re** (2.0 mM) and BIH (0.1 M) after steady-state light irradiation (λ = 480 nm) for 2 min.

of retention time is attributed to **RuC2Re**. After the light irradiation, this peak decreased and a new peak appeared at 3.3 min, which is attributed to a tetracarbonyl complex **RuC2Re(CO)** that has a *fac*-[Re^{I}(diimine)(CO)$_4$]$^+$ unit because of the consistency of the retention time and the absorption spectra with the synthesized **RuC2Re(CO)** (Fig. S10†). After irradiation for 2 h, the accumulation of **RuC2Re(CO)** in the reaction solution was saturated, and, in this stage, approximately 45% of **RuC2Re** was converted to **RuC2Re(CO)** (Fig. 5b). Notably, **RuC2Re(CO)** is fully converted to the carboxylate–ester complex **RuC2Re(CO-TEOA)** in the DMSO–TEOA (5 : 1 v/v) solution (eqn (6)) as presented below. Therefore, in the weak acidic eluent (pH = 5.9), **RuC2Re(CO)** is recovered from **RuC2Re(CO-TEOA)** during the UHPLC analysis, which is the backward reaction of eqn (6). Although Re(I) tetracarbonyl complexes have been proposed as intermediates in the photocatalytic reduction of CO_2 in various systems using *fac*-Re(diimine)(CO)$_3$L type complexes,[26–28,32,62] to the best of our knowledge, this is the first experimental identification of this intermediate in the photocatalytic reaction for CO_2 reduction.

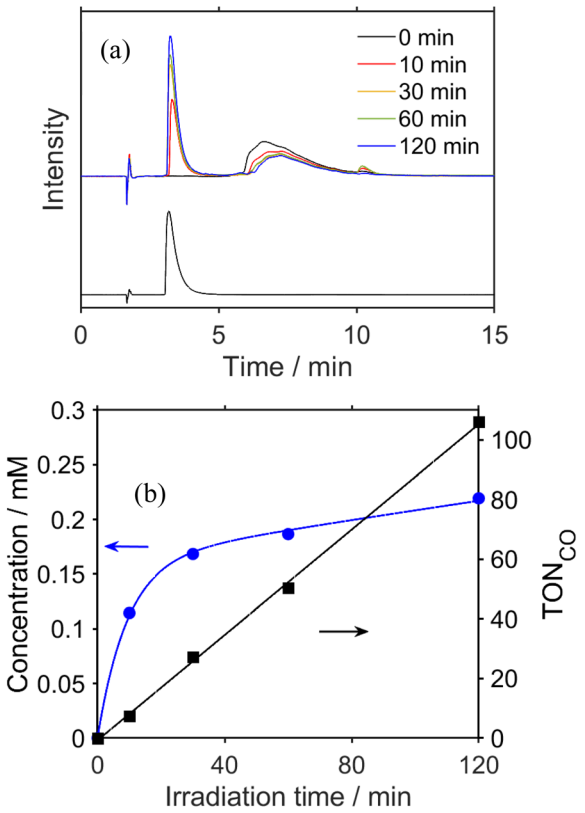

Fig. 5 (a) UHPLC chromatograms of (top) a CO_2 saturated DMSO–TEOA (5 : 1 v/v) solution containing **RuC2Re** (0.5 mM) and BIH (0.1 M) before and after irradiation at 490–620 nm (λ_{max} = 530 nm) for various irradiation times; the chromatogram of a DMSO–TEOA (5 : 1 v/v) solution containing **RuC2Re(CO)** is shown at the bottom (ODS; eluent: MeOH–KH_2PO_4 buffer (pH = 5.9); detection wavelength λ_{det} = 460 nm). (b) Concentration change of the accumulated **RuC2Re(CO-TEOA)**, which was observed as **RuC2Re(CO)** in the UHPLC analysis (blue) and TON of CO formation (black) during irradiation.

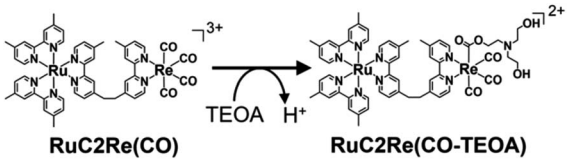

(6)

Kubiak *et al.* reported that the one-electron reduction of the Re(I) diimine tetracarbonyl complex caused the rapid release of one of the CO ligands from the reduced complex.[62] However, a significant amount of "**RuC2Re(CO)**" was detected in the UHPLC analysis of the photocatalytic reaction solution as described above even though the Re(I) diimine tetracarbonyl complexes could be easily reduced compared to the Re(I) diimine tricarbonyl complexes owing to the electron withdrawing properties of the CO ligand, *e.g.*, E([Re(dmb)(CO)$_4$]$^+$/[Re(dmb$^{\bullet-}$)(CO)$_4$]) = − 1.44 V *vs.* Ag/AgNO$_3$ which is +160 mV more positive than the first reduction potential of **Re** (Fig. S11†).[46] This accumulation is understandable because, in the photocatalytic reaction solution, the produced **RuC2Re(CO)** rapidly reacts with TEOA to yield **RuC2Re(CO-TEOA)** (eqn (6)) with a reduction potential that is more negative than that of **RuC2Re(CO)** as described below. **RuC2Re(CO)** showed four vibration bands of the CO ligands at 2119, 2024, 1997, and 1955 cm^{-1} in DMSO (Fig. 6, blue line). In the DMSO–TEOA (5 : 1 v/v) solution, on the other hand, these vibration bands were not observed at all, and another spectrum attributable to a tricarbonyl Re(I) complex was observed at ν_{CO} = 2006, 1895 (br) cm^{-1} (Fig. 6, red line), with a spectral change that is attributed to the addition of the deprotonated TEOA to one of the CO ligands of **RuC2Re(CO)** producing **RuC2Re(CO-TEOA)**. Several similar reactions were reported, in which the nucleophilic attack of some bases such as OH$^-$ and OMe$^-$ to tetracarbonyl Re(I) complexes efficiently proceeded to form the corresponding carboxylate (ester) complexes.[39,63] The addition of TEOA to the CO ligand of the [Ru(diimine)$_2$(CO)$_2$]$^{2+}$-type complexes was also reported.[64,65] It should be noted that **RuC2Re(CO-TEOA)** has the same ν_{CO}s as those of the long-lived intermediate observed by the TR-IR measurement (Fig. 1b and 6). This also supports the observation that the long-lived intermediate in the TR-IR measurement is **RuC2Re(CO-TEOA)**. It is expected that most of the

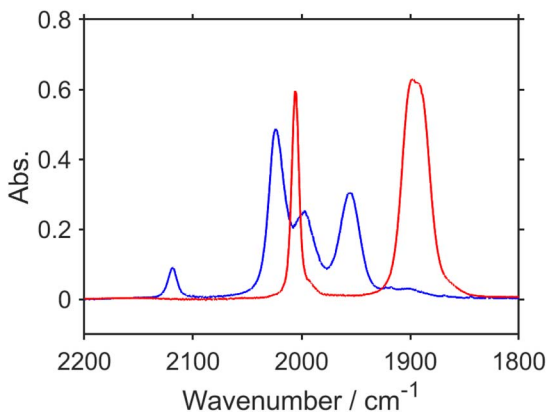

Fig. 6 FT-IR spectra of **RuC2Re(CO)** (3 mM) measured in a DMSO (blue) or DMSO–TEOA (5 : 1 v/v) (red) solution; d = 0.5 mm.

produced **RuC2Re(COOH)** is converted to **RuC2Re** or **RuC2Re(CO-TEOA)** during the time (1–2 min) between the stopping of the light irradiation and the start of the UHPLC measurement because the lifetime of **RuC2Re(COOH)** is $k_2^{-1} \sim 30$ s in the dark.

The bimolecular rate constant of the addition of TEOA to **RuC2Re(CO)** was determined to be 4.56 ± 0.03 M^{-1} s^{-1} using the stopped-flow method used for mixing the DMSO–TEOA (5 : 2 v/v) solution ([TEOA] = 2.52 M) with the same volume of DMSO solution containing **RuC2Re(CO)** (0.1 mM), where the addition of TEOA to **RuC2Re(CO)** caused a red shift of the MLCT absorption band of the Re catalyst unit (Fig. S12†). Thus, the reaction rate of this addition reaction is much faster than that of the subsequent reactions of **RuC2Re(COOH)** and **RuC2Re(CO-TEOA)**.

The cyclic voltammogram of the model mononuclear complex, *fac*-[Re(dmb)(CO)$_3${COOCH$_2$CH$_2$N(CH$_2$CH$_2$OH)$_2$}] (**Re(CO-TEOA)**) first showed a reduction potential at $E_{1/2} = -1.72$ V *vs.* Ag/AgNO$_3$ (Fig. S13†), which was −280 mV more negative compared to that of $[Re(dmb)(CO)_4]^+$ ($E_{1/2} = -1.44$ V, Fig. S11†). The reversibility of the first reduction of **Re(CO-TEOA)** decreased at a slower scan rate, suggesting that the reduction of **Re(CO-TEOA)** triggers the change of the carboxylate ester ligand, which releases CO (eqn (7)).

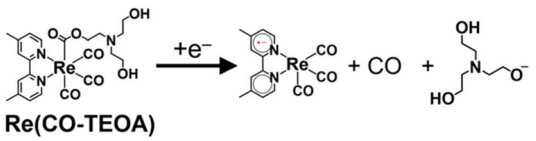

(7)

Fig. S14† shows the differential pulse voltammogram (DPV) of **RuC2Re(CO-TEOA)**. Five reduction waves were observed at $E_p = -1.48$, −1.60, −1.69, −1.80 and −2.03 V *vs.* Ag/AgNO$_3$. The most positive and smallest wave is attributed to the reduction of the solvent complex that is produced by the slow dissociation of the carboxylate ester ligand from **RuC2Re(CO-TEOA)** when preparing for the DPV measurement. The second, fourth, and fifth peaks are attributed to the Ru unit, and only the third peak is derived from the Re carboxylate ester unit, which is close to the first reduction potential of **Re(CO-TEOA)**. Therefore, electron transfer from the one-electron reduced Ru unit to the Re carboxylate ester unit is an endergonic process. The added electron was mainly localized in the Ru unit but not in the Re unit in the one-electron reduced **RuC2Re(CO-TEOA)**. This is the main reason why **RuC2Re(CO-TEOA)** is relatively stable during the photocatalytic reactions. To confirm the CO production from **RuC2Re(CO-TEOA)**, a DMSO–TEOA (5 : 1 v/v) solution containing **RuC2Re(CO-TEOA)** (0.5 mM) and BIH (0.1 M) was irradiated with 490–620 nm LED light ($\lambda_{max} = 530$ nm) under Ar; after 5 min irradiation, **RuC2Re(CO-TEOA)** decreased by 23% and the same amount of CO was produced. The decay of **RuC2Re(CO-TEOA)** was clearly accelerated compared to that in the dark, and its rate increased under irradiation with higher light intensity (Fig. S15†). Although, therefore, the added electron is mainly localized in the Ru unit, the reductive acceleration of CO loss from the one-electron reduced **RuC2Re(CO-TEOA)** more rapidly proceeds compared to that from **RuC2Re(CO-TEOA)** itself.

Discussion

In the TR-IR experiments, the photons were irradiated only for 7 ns and then the following processes occurred without visible-light irradiation. Because the light source used for the actual photocatalytic reaction experiments is not the pulse laser but a steady-state light source such as an LED lamp, light is continuously irradiated to the solution during the photocatalytic reaction. Therefore, the following processes after the excitation of the photosensitiser unit could be partially different between the TR-IR measurements and actual photocatalytic reactions. From this viewpoint, we first focus on the reaction mechanism of the photocatalytic CO_2 reduction in the TR-IR measurements, and then evaluate its difference from that in the actual photocatalytic reactions.

Reaction mechanism of CO_2 reduction under the TR-IR measurement conditions

The rapid scan FT-IR measurements with laser flash photolysis clarified the following.

(i) OERS **RuC2(Re)**$^-$ was quantitatively converted to the carboxylic acid intermediate **RuC2Re(COOH)**. The isotope experiments clearly indicated that the carbon source of the C=O group of the carboxylic acid ligand in **RuC2Re(COOH)** is CO_2. To the best of our knowledge, this is the first experimental detection of a Re(I) carboxylic acid complex as an intermediate that is produced by two-electron reduction of the *fac*-[Re(diimine)(CO)$_3$L]$^{n+}$-type complex during photocatalytic reactions.[25,27,28,35,36,38–40] The rate of this conversion reaction linearly depends on the concentration of **RuC2(Re)**$^-$ with a rate constant of $k_1 = 1.8$ s^{-1}.

(ii) **RuC2Re(COOH)** changed the structure with $k_2 = (3.1 \pm 0.8) \times 10^{-2}$ s^{-1}. Approximately 40% of **RuC2Re(COOH)** returned to the starting complex **RuC2Re** with the release of CO and OH^- and the addition of CO_2 and a deprotonated TEOA in the dark reaction (Process A in Scheme 3). The pseudo-first order rate constant of the CO_2 capture reaction by the deprotonated TEOA coordinated complex was determined to be 5.2 s^{-1} (Fig. S21†) under a 100% CO_2 atmosphere. Because this rate of the CO_2 capture reaction is two orders of magnitude faster than k_2, the rate determining step of Process A is not by the coordination of the deprotonated TEOA and CO_2 insertion to Re–O bond but by the release of CO and OH^- from **RuC2Re(COOH)**.

(iii) Approximately 60% of **RuC2Re(COOH)** was converted to another long-lived intermediate **RuC2Re(CO-TEOA)** that was produced by the addition of TEOA to the tetracarbonyl complex **RuC2Re(CO)** (Processes B and C in Scheme 3). It was deduced that another CO_2 molecule attacks the O atom of the OH group of *fac*-[Re^I(dmb)(CO)$_3$(COOH)] to form $[Re(dmb)(CO)_4]^+$ and HCO_3^-.[41] During the TR-IR measurements, **RuC2Re(CO-TEOA)** slowly but quantitatively returned to **RuC2Re** with $k_3 = (3.0 \pm 0.6) \times 10^{-3}$ s^{-1} (Process D).

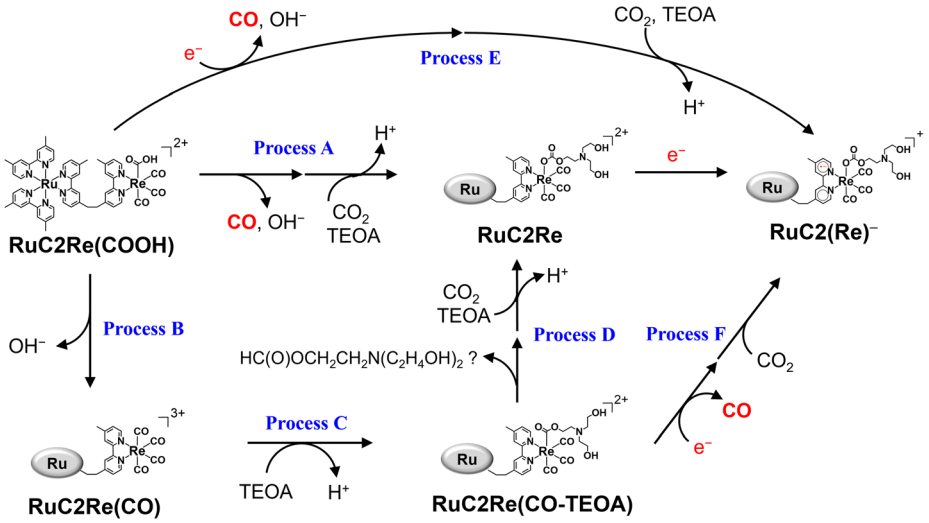

Scheme 3 Subsequent processes of RuC2Re(COOH).

Conversion reaction mechanism from RuC2(Re)$^-$ to RuC2Re(COOH)

RuC2Re required two electrons to be converted to **RuC2Re(-COOH)**. In other words, the one-electron reduced species **RuC2(Re)**$^-$ or the subsequent intermediate made from **RuC2(Re)**$^-$ received one more electron to produce **RuC2Re(-COOH)**, which is the second reduction process in the photocatalytic cycle for CO_2 reduction. Because the rate of this reductive conversion reaction linearly depended on the concentration of **RuC2(Re)**$^-$ with $k_1 = 1.8 \pm 0.1\ s^{-1}$ (Fig. 1 and S5†), the disproportionation reaction of two molecules of **RuC2(Re)**$^-$ was excluded from the subsequent processes of **RuC2(Re)**$^-$. Under the experimental conditions of the TR-IR measurements using the ~7 ns laser pulse, the excitation of **RuC2(Re)**$^-$ and the intermediate could not proceed at a time period of sub-seconds after the laser flash because the interval of the laser pulses was 10 min. Although BI$^\bullet$ has a strong reducing power, it is not the main electron donor to **RuC2(Re)**$^-$ and/or the intermediate because, in the TR-IR measurements, all the produced BI$^\bullet$ passed an electron to **RuC2Re** on the microsecond time scale.[46,66] Therefore, the main second-electron donor to the intermediate (but not to another molecule of **RuC2(Re)**$^-$, *i.e.*, not disproportionation of **RuC2(Re)**$^-$, as described above) was only **RuC2(Re)**$^-$ (and partially **(Ru)**$^-$**C2Re**) in the TR-IR experiments. This is strongly supported by the fact that only a half of the **RuC2Re(COOH)** formed compared to the amount of the decreased **RuC2(Re)**$^-$ and, simultaneously, a half of the bleaching band attributed to the recovery of **RuC2Re** was observed. Based on these results and investigations, we can conclude that the rate determining step in the production processes of **RuC2Re(COOH)** is not the electron transfer (mainly from **RuC2(Re)**$^-$) to another intermediate **RuC2Re(X)** (eqn (9)), but the structure change process of **RuC2(Re)**$^-$ to **RuC2Re(X)** (eqn (8)). After this structure change process, **RuC2Re(X)** accepts one electron from **RuC2(Re)**$^-$ or **(Ru)**$^-$**C2Re** for conversion to **RuC2Re(COOH)**, which is a faster process compared to the structure change.

$$\mathbf{RuC2(Re)^- \xrightarrow{k_1' = 0.9\ s^{-1}} RuC2Re(X)} \quad (8)$$

$$\mathbf{RuC2Re(X) + RuC2(Re)^- \xrightarrow{k >> 0.9\ s^{-1}} RuC2Re(COOH) + RuC2Re} \quad (9)$$

Recently, we reported that the intermediate **Re(X)** produced from the one-electron-reduced mononuclear Re complex **Re**$^-$ has a more positive reduction potential than that of **Re** (−1.6 V *vs.* Ag/AgNO$_3$) and cannot be reduced by the reduced photosensitiser with a reduction potential that is more positive than $E_{1/2}^{red} = -1.4$ V *vs.* Ag/AgNO$_3$.[67] Therefore, the second electron-transfer reaction from **RuC2(Re)**$^-$ to **RuC2Re(X)** is exergonic and, therefore, rapid. Because the decrease of **RuC2(Re)**$^-$ occurs *via* two processes (eqn (8) and (9)), the actual rate constant of the structure change from **RuC2(Re)**$^-$ to **RuC2Re(X)** is a half of k_1 (the decay constant of **RuC2(Re)**$^-$), *i.e.*, $k_1' = 0.9\ s^{-1}$ (eqn (8)). To obtain information on this intermediate **RuC2Re(X)**, we conducted similar TR-IR experiments in a CO_2 saturated DMSO–TEOA (5 : 1 v/v) solution containing NH_4PF_6 (20 mM) as the proton source (Fig. S16†). Under these conditions, the converted reaction of **RuC2(Re)**$^-$ to **RuC2Re(COOH)** ($k_1 = 2.7\ s^{-1}$) was approximately 1.5 times faster than that in the absence of NH_4PF_6. This result suggested that protons are involved in the subsequent process of **RuC2(Re)**$^-$ converting to **RuC2Re(X)**.

We should not be able to obtain the spectral data of **RuC2Re(X)** directly in the photocatalytic reaction because the concentration of **RuC2Re(X)** should be very low owing to the subsequent rapid reduction reaction (eqn (9)). Therefore, we evaluated the mechanism of the conversion reaction of the model mononuclear complex **Re**$^-$ using the DFT calculations based on the experimental results as described above (Schemes 4 and S1†). In the initial process, a hydrogen bond forms between the oxygen atom of the carbonate ester ligand of **Re**$^-$

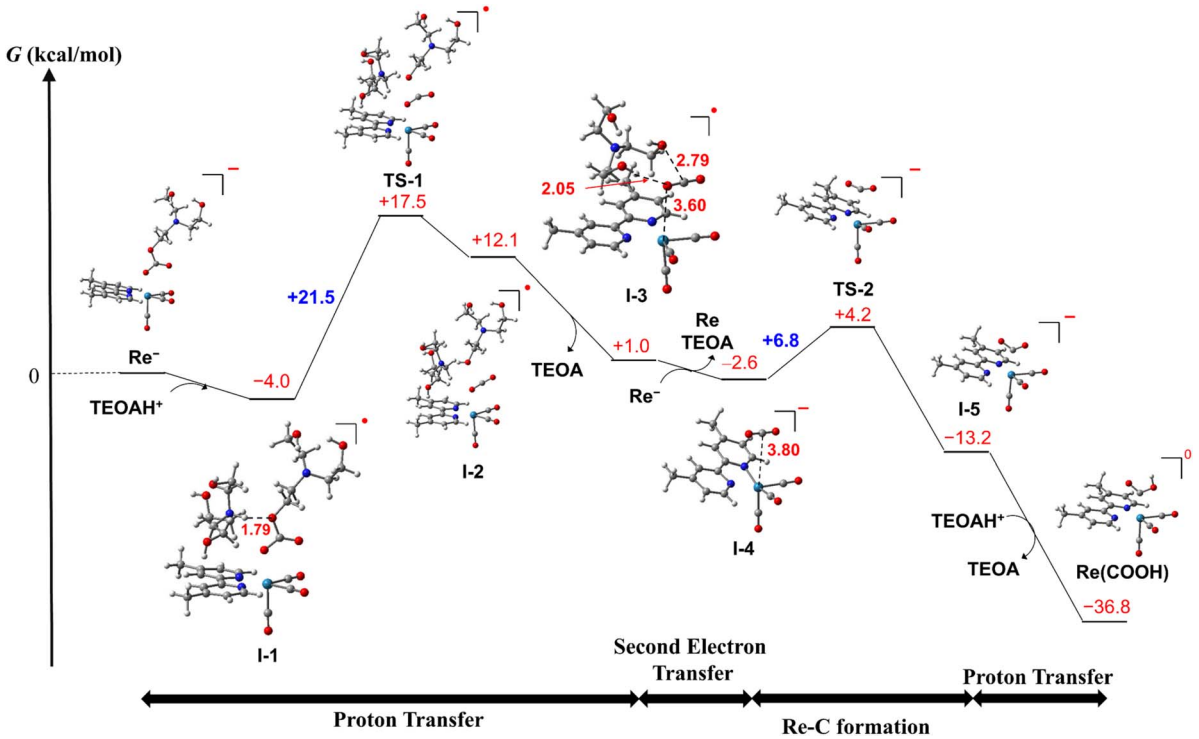

Scheme 4 Computed free energy profile for the conversion reaction from the OERS of *fac*-Re(dmb)(CO)$_3${OC(O)OCH$_2$CH$_2$N(CH$_2$CH$_2$OH)$_2$} (**Re**$^-$) to *fac*-Re(dmb)(CO)$_3$(COOH) (**Re(COOH)**). Re–C bond formation occurs after the second electron reduction.

and a protonated TEOA (tertiary ammonium ion: H–O = 1.79 Å, ΔG° = −4.0 kcal mol^{-1}), *i.e.*, formation of **I-1**, and then the proton transfer from the N^{TEOAH^+} to the O^{TEOA} atom of the carbonate ester ligand that coordinates to the Re center to cleave the C–O^{TEOA} bond of the carbonate ester ligand *via* **TS-1** ($\Delta G^\ddagger$ = +21.5 kcal mol^{-1}). As a result, an intermediate **I-2** is formed (ΔG° = +16.1 kcal mol^{-1}) and is favorably converted to **I-3** (ΔG° = −11.1 kcal mol^{-1}), in which CO_2, previously involved in the carbonate ester bond, forms a weak coordination bond with the Re center *via* one of the O atoms (Re–O = 3.60 Å, ∠O=C=O = 177°) and the dissociated TEOA interacts with CO_2 (O–C = 2.79 Å, H–O = 2.05 Å). There are two plausible subsequent processes of **I-3** as follows.

(1) As shown in Scheme 4, **I-3** favorably accepts an electron before the Re–C bond formation to form the two-electron reduced species **I-4** (ΔG° = −3.6 kcal mol^{-1} in the calculation using **Re**$^-$ as the electron donor), in which the Re center is weakly coordinated with CO_2 *via* the C atom (Re–O = 3.80 Å, ∠O=C=O = 178°). **I-4** is readily converted to the C-coordinated CO_2 adduct **I-5** *via* **TS-2** (ΔG° = −10.6 kcal mol^{-1}, $\Delta G^\ddagger$ = +6.8 kcal mol^{-1}). This reaction is thermodynamically more favorable than the CO_2 cleavage in **I-4**, *i.e.*, the dissociation of CO_2 from the Re center (ΔG° = −3.3 kcal mol^{-1}).

(2) The formation processes of **I-3** are the same as in Scheme 4. As shown in Scheme S1,† **I-3** is converted to Re(dmb)(CO)$_3$(-CO_2) (**I-4′**) with the Re–C bond *via* **TS-2′** (ΔG° = +3.4 kcal mol^{-1}, $\Delta G^\ddagger$ = +7.1 kcal mol^{-1}), and then **I-4′** accepts an electron, forming the two-electron reduced species **I-5** (ΔG° = −17.7 kcal mol^{-1} (=−770 meV)).

On one hand, the calculated reduction potential of **I-4′** is 770 mV more positive than that of **Re**. On the other hand, because the calculated reduction potential of **I-3** is +160 mV more positive than that of **Re**, which is consistent with the experimental results described above,[67] the mechanism shown in Scheme 4 is more reliable.

Protonation of **I-5** produces the carboxylic acid complex **Re(COOH)** (ΔG° = −23.6 kcal mol^{-1}). These calculations suggest that the rate-determining step in the conversion reaction from **Re**$^-$ to **Re(COOH)** is the proton transfer *via* **TS-1**, which is consistent with the experimental observations, *i.e.*, the addition of the proton source accelerated the conversion rate of **RuC2(Re)**$^-$ to **Re(COOH)**. Based on these results and investigations, it can be inferred that the structure of the Re unit in the experimentally unobservable intermediate **RuC2Re(X)** that accepts the second electron is the CO_2 coordination complex **I-3** (Scheme 4).

Electron donor for the second reduction process and role of RuC2Re(CO-TEOA) in the actual photocatalytic CO_2 reduction reaction

Fig. 5b shows that the concentrations of the metal complexes such as **RuC2Re** and **RuC2Re(CO-TEOA)** drastically changed during the photocatalytic reactions for the CO_2 reduction using the steady-state light. Their concentrations were different from that observed in the TR-IR measurement, and changed depending on the light intensity of the irradiation. The starting complex **RuC2Re** and the relatively stable intermediates, *i.e.*, **RuC2Re(COOH)** and **RuC2Re(CO-TEOA)**, absorb light during

the photocatalytic reactions whereas, in the TR-IR measurements using the pulse laser, only **RuC2Re** is excited even though the light flux of the laser pulse is much higher than that of the steady-state irradiation. Therefore, we reconsidered the role of the accumulated intermediates as the "external" redox photosensitisers which might supply an electron to the intermediate **RuC2Re(X)** in the second reduction process, and the CO release mechanism as well.

The detected **RuC2Re(CO-TEOA)** could be one of the intermediates that produce CO during the photocatalytic reaction. The TR-IR measurement indicated that **RuC2Re(CO-TEOA)** slowly returned to **RuC2Re** under dark conditions with $k_3 = (3.0 \pm 0.6) \times 10^{-3}$ s^{-1} (Fig. 1b and 3). To confirm CO production by this reaction (Process D in Scheme 3), the gas and liquid phases of a sealed 11 mL sample tube, which included a CO_2 saturated DMSO–TEOA (5 : 1 v/v) solution (1 mL) containing **RuC2Re(CO-TEOA)** (0.5 mM) and BIH (0.1 M), were analyzed by GC and UHPLC respectively. In the dark, no CO was formed even though **RuC2Re(CO-TEOA)** was converted to **RuC2Re**. Although we could not identify the product from the carboxylate ester ligand, it could be the carboxylate ester (formate ester) itself, $N(CH_2CH_2OH)_2(CH_2CH_2OCHO)$.

How about the photochemical reaction of **RuC2Re(CO-TEOA)** during the photocatalytic reaction? The decay of **RuC2Re(CO-TEOA)** was accelerated during irradiation in the presence of BIH compared to that in the dark; the photochemical reaction rate increased under irradiation with a higher light intensity (Fig. S15†). The amount of CO detected was similar to the decreased amount of **RuC2Re(CO-TEOA)** in the photochemical reaction. These results indicate that the OERS of **RuC2Re(CO-TEOA)** ($[$**RuC2Re(CO-TEOA)**$]^-$), which was produced *via* photochemical electron transfer from BIH to the excited Ru photosensitiser unit of **RuC2Re(CO-TEOA)** or reduction of ground state **RuC2Re(CO-TEOA)** by $BI^\bullet$, quantitatively releases CO (Process F in Scheme 3). It should be noted that this photochemical CO production from **RuC2Re(CO-TEOA)** ($\sim$0.052 min^{-1}) was much slower than the CO formation during the photocatalytic CO_2 reduction using **RuC2Re** with the same light intensity (TOF_{CO} = 0.88 min^{-1}, Fig. 5). As shown in Fig. 5b, a certain amount of **RuC2Re** (the initial concentration was 0.5 mM) was converted to **RuC2Re(CO-TEOA)** in the initial stage of the photocatalytic reduction; 0.22 mM **RuC2Re(CO-TEOA)** was accumulated in the photocatalytic reaction solution after irradiation for 120 min. The concentration of **RuC2Re(CO-TEOA)** rapidly increased in the first stage of the photocatalytic reaction, and then almost stabilized until 120 min of irradiation. A comprehensive evaluation of these results indicates that the CO release from $[$**RuC2Re(CO-TEOA)**$]^-$ during the photocatalytic reaction (Processes B, C and F in Scheme 3) is not the primary pathway of the photocatalytic CO_2 reduction using **RuC2Re** because its reaction rate was too slow as described above (Fig. S15†) and the continuous and stable formation of CO was already observed 10 min after the irradiation started, and then continued until 2 h of irradiation even though the concentrations of **RuC2Re** and **RuC2Re(CO-TEOA)** were changed in the initial stage of the photocatalytic reaction (Fig. 5). Therefore, the main process of the subsequent reactions of **RuC2Re(COOH)** in the photocatalytic reactions was the direct formation of CO from **RuC2Re(COOH)** (Process A).

It is reasonable to deduce that not only $[$**RuC2(Re)**$]^-$ but also $[$**RuC2Re(CO-TEOA)**$]^-$ worked as the electron donor because a considerable amount of **RuC2Re(CO-TEOA)** was accumulated in the reaction solution during the photocatalytic reactions (Fig. 5). The excited state of **RuC2Re(CO-TEOA)** had a lifetime that was long enough and the excited state of its Ru unit was efficiently quenched by BIH. Because the reduction potential of the Re unit of **RuC2Re(CO-TEOA)** is 90 mV more negative than that of the Ru unit, the added electron to **RuC2Re(CO-TEOA)** is mainly localized at the Ru unit. The role of $[$**RuC2Re(CO-TEOA)**$]^-$ as the electron donor not only to **RuC2Re(X)** but also to the starting complex **RuC2Re** causes a longer lifetime of **RuC2Re(CO-TEOA)** in the steady-state irradiation. Thus, the accumulated **RuC2Re(CO-TEOA)** not only works as the precursor of CO formation after its reduction but also as an "external" redox photosensitiser in the photocatalytic reaction. This was the main reason why the larger amount of **RuC2Re(CO-TEOA)** was accumulated during the steady-state irradiation (Fig. 5).[46]

On the other hand, $BI^\bullet$ should not be the main electron donor of the second reduction in the photocatalytic reactions because the concentration of the intermediate **RuC2Re(X)** was much lower than that of the other complexes such as **RuC2Re**, **RuC2Re(COOH)** and **RuC2Re(CO-TEOA)** that could accept electrons from $BI^\bullet$ during the photocatalytic reactions. The excitation of $[$**RuC2(Re)**$]^-$ and/or **RuC2Re(X)** followed by reductive quenching with BIH had very low possibilities as a second reduction process because of the low flux of photons and low concentration of $[$**RuC2(Re)**$]^-$ and **RuC2Re(X)** under the photocatalytic reaction conditions. For example, in the reported quantum yield measurements of **RuC2Re**,[46] the number of photons absorbed by the Ru photosensitiser unit was 3.7×10^{-9} einstein s^{-1} (480 nm), and the amount of the Ru photosensitiser unit was 0.2 μmol in the solution. This indicates that one Ru photosensitiser unit can absorb one photon every 53 s on average. Therefore, the lifetimes of $[$**RuC2(Re)**$]^-$ (k_1^{-1} = 0.56 s) and **RuC2Re(X)** ($\ll$0.56 s) are too short for these intermediates to absorb a photon. Additionally, excitation of the Ru unit of $[$**RuC2(Re)**$]^-$ caused not only reductive quenching by BIH but also intramolecular reductive quenching from the one-electron reduced Re unit to the excited state of the Ru unit, which was followed by rapid intramolecular back electron transfer.[68]

CO release process from RuC2Re(COOH)

RuC2Re(COOH) exhibited a comparatively prolonged lifetime in the dark and had two conversion processes (Processes A and B in Scheme 3). The dominant process for CO production is Process A (k = 0.03 s^{-1} in the dark) as described above in the TR-IR measurements. If the CO-release process from **RuC2Re(-COOH)** was only the dark reaction, it would become the rate-determining step of the photocatalytic CO_2 reduction under higher light intensity. However, under irradiation using a strong LED-light (λ_{ex} = 440–600 nm), which was the strongest light intensity in our laboratory, the turnover frequency of the photocatalytic CO formation (TOF_{CO}) was up to $k = 0.4$ s^{-1} (Fig. S17†), which was much faster than the CO-release reactions of **RuC2Re(COOH)** in the dark. It is noteworthy that the rate of the subsequent reaction of **RuC2Re(COOH)** (Process A) (k = 0.03

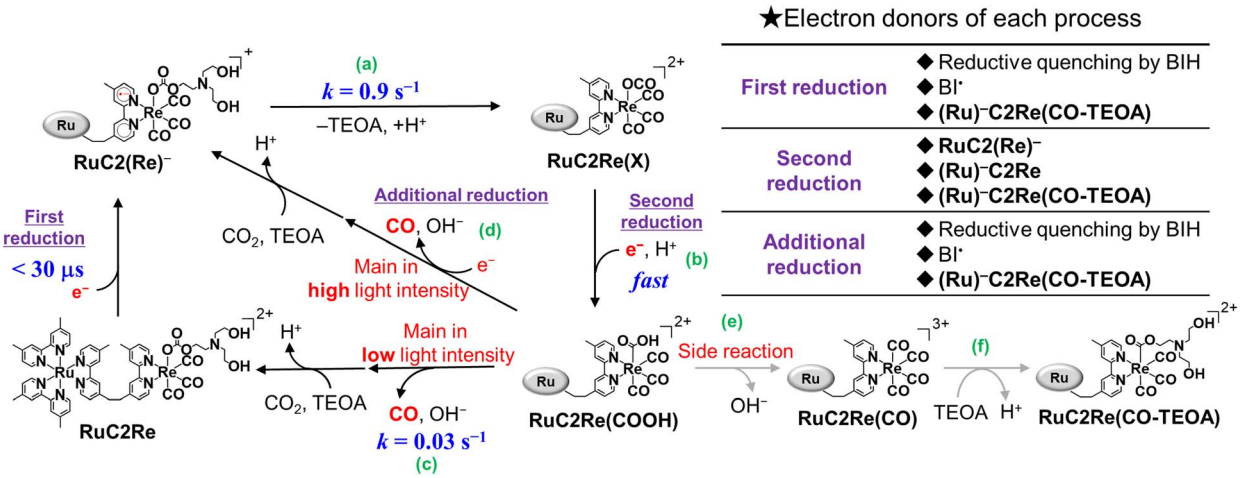

Scheme 5 Full reaction mechanism of photocatalytic CO_2 reduction by using **RuC2Re** and BIH.

s^{-1}) was measured in the TR-IR experiments after laser irradiation or just after cutting steady-light irradiation (Fig. 1b and S9†), particularly, without irradiation. The "unexpected" faster reaction rates of CO formation in the photocatalytic reaction originated from photochemical reduction and/or reduction of the accumulated **RuC2Re(COOH)** (Process E). The accumulation of **RuC2Re(COOH)** enabled not only the photochemical reduction of **RuC2Re(COOH)** but also its reduction by BI$^{\bullet}$ and/or the one-electron-reduced form of **RuC2Re(CO-TEOA)**. It was deduced that the reduced Re^0 carboxylic acid complexes $[Re^0(bpy)(CO)_3(COOH)]^-$ were converted to the corresponding $[Re^0(bpy)(CO)_4]^0$ and released CO.[25,32,62]

Fig. S18† shows the CV of **Re(COOH)** in an Ar purged DMSO–TEOA (5 : 1 v/v) solution. **Re(COOH)** exhibits a chemically irreversible reduction wave at $E_{1/2} = -1.73$ V *vs.* $Ag/AgNO_3$ and a reoxidation wave at $E_p = -1.53$ V, which is assigned to the one-electron reduced DMSO and/or TEOA coordinated complex produced after the CO release reaction from the one-electron reduced **Re(COOH)**. From these results and investigations, under high light-intensity conditions, the reduction of **RuC2Re(COOH)** and the subsequent CO release from the reduced complex was one of the main CO-formation pathways in the photocatalytic reaction. Fig. S19† shows the UV-vis absorption spectrum changes of a photocatalytic reaction solution containing **RuC2Re** (0.05 mM) and BIH (0.1 M) during steady-state light irradiation with a relatively high light intensity ($\lambda_{ex} = 480$ nm, 2.6×10^{-8} einstein s^{-1}). Under these conditions, the Ru unit can absorb a photon every 11 s on average. The absorption band appeared at 515 nm in the initial stage of the photocatalytic reaction. This absorption band is assigned to the one-electron reduced species of **RuC2Re**, *i.e.*, the equilibrium mixture of **(Ru)$^-$C2Re** and **RuC2(Re)$^-$**. After more than 60 s of light irradiation, the shape of the absorption band drastically changed to that at $\lambda_{max} = 510$ and 535 nm, which is consistent with the absorption of the one-electron reduced species of $[Ru(dmb)_3]^{2+}$.[46,66] This spectral change clearly indicates the formation of **(Ru)$^-$C2Re(COOH)** (and partially **(Ru)$^-$C2Re(CO-TEOA)**) in which the Re unit has a more negative reduction potentials compared to the Ru unit.[69] Although the electron transfer from the one-electron-reduced Ru unit to the Re carboxylic acid unit is endergonic, the CO release reaction from the one-electron reduced **RuC2Re(COOH)** should proceed because of the irreversibility of the one-electron reduced Re carboxylic acid complex.

It should be interesting to investigate another photocatalytic system using 1-benzyl-1,4-dihydronicotinamide (BNAH) that can donate only one electron instead of BIH that donates two electrons. It was reported that the maximum TOF_{CO} was 0.078 s^{-1} when BNAH was used as the sacrificial electron donor.[70] This was close to the rate of the CO release reaction from **RuC2Re(COOH)** ($k = 0.03$ s^{-1}) probably because the reduction process of **RuC2Re(COOH)** was much slower compared to the system using BIH. These deductions clearly indicate that the rate-determining step of the photocatalytic CO_2 reduction by the Ru(II)–Re(I) supramolecular photocatalysts strongly depends on the reaction conditions, *i.e.*, light intensity, type of sacrificial electron donor, and concentration of the photocatalyst.

It is noteworthy that the pseudo-first-order rate constant of the CO_2 capture reaction under the 100% CO_2 atmosphere (5.2 s^{-1}) was above 10 times faster than the highest TOF_{CO} using high light intensity (0.4 s^{-1}) (Fig. S21†). This result clearly indicates that the CO_2 capture reaction is not a rate determining step of the photocatalytic reduction of CO_2. This is one of the reasons why the Ru(II)–Re(I) supramolecular photocatalyst exhibits excellent photocatalytic activity even under a low-concentration CO_2 atmosphere.[6]

Conclusions

The overall reaction mechanism of the photocatalytic reduction of CO_2 using **RuC2Re** consisting of the $[Ru(diimine)_3]^{2+}$ photosensitiser and the *fac*-$[Re(diimine)(CO)_3\{OC(O)OCH_2CH_2NR_2\}]$ catalyst units was elucidated as shown in Scheme 5.

The carboxylic acid complex **RuC2Re(COOH)** was detected as a subsequent intermediate of the one-electron reduced species (OERS) **RuC2(Re)$^-$** by time-resolved IR (TR-IR) measurements

using rapid-scan FT-IR spectroscopy with laser flash photolysis as well as in the actual photocatalytic reaction using steady-state irradiation. The kinetic analysis of the TR-IR spectra and DFT calculations revealed that the Re unit of **RuC2Re**$^-$ changes its structure to a CO_2-coordinated complex (Process (a)), and then accepts an additional electron from another OERS to form **RuC2Re(COOH)** (Process (b)).

There were two conversion processes of **RuC2Re(COOH)**. The main process involved the release of CO and OH^-, and **RuC2Re** was recovered without forming any other long-lived intermediate (Process (c)). Under the actual photocatalytic reaction conditions, especially when the light intensity was high, **RuC2Re(COOH)** was reduced by photoinduced electron transfer and by BI$^\bullet$ to accelerate the release of CO (Process (d)). As a side reaction, **RuC2Re(COOH)** released only OH^- to form a tetracarbonyl species, **RuC2Re(CO)** (Process (e)), that was rapidly converted to the carboxylate ester complex **RuC2Re(CO-TEOA)** by the nucleophilic attack of TEOA (Process (f)). **RuC2Re(CO-TEOA)** has a relatively long lifetime, but the reduction of **RuC2Re(CO-TEOA)** induces the release of CO from this intermediate. **RuC2Re(CO-TEOA)** serves not only as the precursor for CO formation but also as an external redox photosensitiser in the photocatalytic reaction.

Data availability

All the data supporting this article have been included in the main text and the ESI.†

Author contributions

Kei Kamogawa: most of the experiments and calculations, discussion, writing the manuscript. Yuki Kato and Takumi Noguchi: TR-IR measurements using the rapid scan FT-IR method, discussion, writing the manuscript. Koichi Nozaki: calculations, discussion. Yusuke Tamaki: some experiments, discussion. Tatsuo Nakagawa: experiments using the stopped flow method. Osamu Ishitani: planning the research, discussion, collecting the research, writing the manuscript.

Conflicts of interest

There are no conflicts to declare.

Acknowledgements

This work was supported by JSPS KAKENHI under Grant Number JP20H00396. K. K. acknowledges the financial support from the JSPS Fellowship for Young Scientists (JP22KJ1330). We thank Ms. Kumiko Koyama and Mr Kido Okamoto for their help in the stopped flow experiments. DFT calculations were performed on a TSUBAME3.0 supercomputer at the Tokyo Institute of Technology, supported by the MEXT Project of the Tokyo Tech Academy for Convergence of Materials and Informatics (TAC-MI).

Notes and references

1 Y. Kuramochi, O. Ishitani and H. Ishida, *Coord. Chem. Rev.*, 2018, **373**, 333–356.
2 E. Boutin, L. Merakeb, B. Ma, B. Boudy, M. Wang, J. Bonin, E. Anxolabéhère-Mallart and M. Robert, *Chem. Soc. Rev.*, 2020, **49**, 5772–5809.
3 J. Hawecker, J.-M. Lehn and R. Ziessel, *J. Chem. Soc., Chem. Commun.*, 1983, 536–538.
4 J. Hawecker, J.-M. Lehn and R. Ziessel, *Helv. Chim. Acta*, 1986, **69**, 1990–2012.
5 T. Morimoto, T. Nakajima, S. Sawa, R. Nakanishi, D. Imori and O. Ishitani, *J. Am. Chem. Soc.*, 2013, **135**, 16825–16828.
6 T. Nakajima, Y. Tamaki, K. Ueno, E. Kato, T. Nishikawa, K. Ohkubo, Y. Yamazaki, T. Morimoto and O. Ishitani, *J. Am. Chem. Soc.*, 2016, **138**, 13818–13821.
7 A. M. Cancelliere, F. Puntoriero, S. Serroni, S. Campagna, Y. Tamaki, D. Saito and O. Ishitani, *Chem. Sci.*, 2020, **11**, 1556–1563.
8 Y. Kuramochi, J. Itabashi, K. Fukaya, A. Enomoto, M. Yoshida and H. Ishida, *Chem. Sci.*, 2015, **6**, 3063–3074.
9 Y. Kuramochi, K. Fukaya, M. Yoshida and H. Ishida, *Chem.–Eur. J.*, 2015, **21**, 10049–10060.
10 Z. Guo, S. Cheng, C. Cometto, E. Anxolabehere-Mallart, S. M. Ng, C. C. Ko, G. Liu, L. Chen, M. Robert and T. C. Lau, *J. Am. Chem. Soc.*, 2016, **138**, 9413–9416.
11 L. Chen, Y. Qin, G. Chen, M. Li, L. Cai, Y. Qiu, H. Fan, M. Robert and T.-C. Lau, *Dalton Trans.*, 2019, **48**, 9596–9602.
12 H. Rao, L. C. Schmidt, J. Bonin and M. Robert, *Nature*, 2017, **548**, 74–77.
13 H. Rao, C. H. Lim, J. Bonin, G. M. Miyake and M. Robert, *J. Am. Chem. Soc.*, 2018, **140**, 17830–17834.
14 A. Call, M. Cibian, K. Yamamoto, T. Nakazono, K. Yamauchi and K. Sakai, *ACS Catal.*, 2019, **9**, 4867–4874.
15 X. Zhang, K. Yamauchi and K. Sakai, *ACS Catal.*, 2021, **11**, 10436–10449.
16 Z. Guo, G. Chen, C. Cometto, B. Ma, H. Zhao, T. Groizard, L. Chen, H. Fan, W.-L. Man, S.-M. Yiu, K.-C. Lau, T.-C. Lau and M. Robert, *Nat. Catal.*, 2019, **2**, 801–808.
17 T. Ouyang, H. H. Huang, J. W. Wang, D. C. Zhong and T. B. Lu, *Angew Chem. Int. Ed. Engl.*, 2017, **56**, 738–743.
18 T. Ouyang, H.-J. Wang, H.-H. Huang, J.-W. Wang, S. Guo, W.-J. Liu, D.-C. Zhong and T.-B. Lu, *Angew. Chem., Int. Ed.*, 2018, **57**, 16480–16485.
19 V. S. Thoi, N. Kornienko, C. G. Margarit, P. Yang and C. J. Chang, *J. Am. Chem. Soc.*, 2013, **135**, 14413–14424.
20 D. Hong, Y. Tsukakoshi, H. Kotani, T. Ishizuka and T. Kojima, *J. Am. Chem. Soc.*, 2017, **139**, 6538–6541.
21 D. Hong, T. Kawanishi, Y. Tsukakoshi, H. Kotani, T. Ishizuka and T. Kojima, *J. Am. Chem. Soc.*, 2019, **141**, 20309–20317.
22 H. Takeda, H. Koizumi, K. Okamoto and O. Ishitani, *Chem. Commun.*, 2014, **50**, 1491–1493.
23 H. Takeda, H. Kamiyama, K. Okamoto, M. Irimajiri, T. Mizutani, K. Koike, A. Sekine and O. Ishitani, *J. Am. Chem. Soc.*, 2018, **140**, 17241–17254.

24 M. L. Clark, P. L. Cheung, M. Lessio, E. A. Carter and C. P. Kubiak, *ACS Catal.*, 2018, **8**, 2021–2029.
25 M. D. Sampson, J. D. Froehlich, J. M. Smieja, E. E. Benson, I. D. Sharp and C. P. Kubiak, *Energy Environ. Sci.*, 2013, **6**, 3748–3755.
26 T. W. Schneider, M. Z. Ertem, J. T. Muckerman and A. M. Angeles-Boza, *ACS Catal.*, 2016, **6**, 5473–5481.
27 Y. Kou, Y. Nabetani, D. Masui, T. Shimada, S. Takagi, H. Tachibana and H. Inoue, *J. Am. Chem. Soc.*, 2014, **136**, 6021–6030.
28 Y. Kou, Y. Nabetani, R. Nakazato, N. V. Pratheesh, T. Sato, S. Nozawa, S.-i. Adachi, H. Tachibana and H. Inoue, *J. Catal.*, 2022, **405**, 508–519.
29 J. Agarwal, B. C. Sanders, E. Fujita, H. F. Schaefer 3rd, T. C. Harrop and J. T. Muckerman, *Chem. Commun.*, 2012, **48**, 6797–6799.
30 K. T. Ngo, M. McKinnon, B. Mahanti, R. Narayanan, D. C. Grills, M. Z. Ertem and J. Rochford, *J. Am. Chem. Soc.*, 2017, **139**, 2604–2618.
31 C. Riplinger and E. A. Carter, *ACS Catal.*, 2015, **5**, 900–908.
32 J. A. Keith, K. A. Grice, C. P. Kubiak and E. A. Carter, *J. Am. Chem. Soc.*, 2013, **135**, 15823–15829.
33 M. H. Ronne, D. Cho, M. R. Madsen, J. B. Jakobsen, S. Eom, E. Escoude, H. C. D. Hammershoj, D. U. Nielsen, S. U. Pedersen, M. H. Baik, T. Skrydstrup and K. Daasbjerg, *J. Am. Chem. Soc.*, 2020, **142**, 4265–4275.
34 F. Wang, B. Cao, W.-P. To, C.-W. Tse, K. Li, X.-Y. Chang, C. Zang, S. L.-F. Chan and C.-M. Che, *Catal. Sci. Technol.*, 2016, **6**, 7408–7420.
35 B. Mondal, A. Rana, P. Sen and A. Dey, *J. Am. Chem. Soc.*, 2015, **137**, 11214–11217.
36 S. Amanullah, P. Saha and A. Dey, *J. Am. Chem. Soc.*, 2021, **143**, 13579–13592.
37 R. Francke, B. Schille and M. Roemelt, *Chem. Rev.*, 2018, **118**, 4631–4701.
38 D. H. Gibson and X. Yin, *J. Am. Chem. Soc.*, 1998, **120**, 11200–11201.
39 D. H. Gibson, X. Yin, H. He and M. S. Mashuta, *Organometallics*, 2003, **22**, 337–346.
40 Y. Hu, F. Zhan, Q. Wang, Y. Sun, C. Yu, X. Zhao, H. Wang, R. Long, G. Zhang, C. Gao, W. Zhang, J. Jiang, Y. Tao and Y. Xiong, *J. Am. Chem. Soc.*, 2020, **142**, 5618–5626.
41 J. Agarwal, E. Fujita, H. F. Schaefer III and J. T. Muckerman, *J. Am. Chem. Soc.*, 2012, **134**, 5180–5186.
42 Y. Hayashi, S. Kita, B. S. Brunschwig and E. Fujita, *J. Am. Chem. Soc.*, 2003, **125**, 11976–11987.
43 Y. Kuramochi, R. Sato, H. Sakuma and A. Satake, *Chem. Sci.*, 2022, **13**, 9861–9879.
44 S. Sato, K. Koike, H. Inoue and O. Ishitani, *Photochem. Photobiol. Sci.*, 2007, **6**, 454–461.
45 B. Gholamkhass, H. Mametsuka, K. Koike, T. Tanabe, M. Furue and O. Ishitani, *Inorg. Chem.*, 2005, **44**, 2326–2336.
46 K. Kamogawa, Y. Shimoda, K. Miyata, K. Onda, Y. Yamazaki, Y. Tamaki and O. Ishitani, *Chem. Sci.*, 2021, **12**, 9682–9693.
47 K. Kamogawa, A. Santoro, A. M. Cancelliere, Y. Shimoda, K. Miyata, K. Onda, F. Puntoriero, S. Campagna, Y. Tamaki and O. Ishitani, *ACS Catal.*, 2023, **13**, 9025–9032.
48 T. Nakagawa, K. Okamoto, H. Hanada and R. Katoh, *Opt. Lett.*, 2016, **41**, 1498–1501.
49 T. Mukuta, S. I. Tanaka, A. Inagaki, S.-Y. Koshihara and K. Onda, *ChemistrySelect*, 2016, **1**, 2802–2807.
50 T. Mukuta, N. Fukazawa, K. Murata, A. Inagaki, M. Akita, S. I. Tanaka, S.-Y. Koshihara and K. Onda, *Inorg. Chem.*, 2014, **53**, 2481–2490.
51 T. Mukuta, P. V. Simpson, J. G. Vaughan, B. W. Skelton, S. Stagni, M. Massi, K. Koike, O. Ishitani and K. Onda, *Inorg. Chem.*, 2017, **56**, 3404–3413.
52 DMSO was used as the solvent because the C=O vibrational band can be observed in this solvent but cannot in DMF or DMA solvent.
53 K. Koike, D. C. Grills, Y. Tamaki, E. Fujita, K. Okubo, Y. Yamazaki, M. Saigo, T. Mukuta, K. Onda and O. Ishitani, *Chem. Sci.*, 2018, **9**, 2961–2974.
54 Y. Yamazaki, K. Ohkubo, D. Saito, T. Yatsu, Y. Tamaki, S. Tanaka, K. Koike, K. Onda and O. Ishitani, *Inorg. Chem.*, 2019, **58**, 11480–11492.
55 J. M. Smieja and C. P. Kubiak, *Inorg. Chem.*, 2010, **49**, 9283–9289.
56 K. Ohkubo, Y. Yamazaki, T. Nakashima, Y. Tamaki, K. Koike and O. Ishitani, *J. Catal.*, 2016, **343**, 278–289.
57 E. Kato, H. Takeda, K. Koike, K. Ohkubo and O. Ishitani, *Chem. Sci.*, 2015, **6**, 3003–3012.
58 H. Takeda, K. Koike, H. Inoue and O. Ishitani, *J. Am. Chem. Soc.*, 2008, **130**, 2023–2031.
59 J. J. Snellenburg, S. Laptenok, R. Seger, K. M. Mullen and I. H. M. van Stokkum, *Journal of Statistical Software*, 2012, **49**, 1–22.
60 I. H. M. van Stokkum, D. S. Larsen and R. van Grondelle, *Biochim. Biophys. Acta, Bioenerg.*, 2004, **1657**, 82–104.
61 C. W. Machan, S. A. Chabolla, J. Yin, M. K. Gilson, F. A. Tezcan and C. P. Kubiak, *J. Am. Chem. Soc.*, 2014, **136**, 14598–14607.
62 K. A. Grice, N. X. Gu, M. D. Sampson and C. P. Kubiak, *Dalton Trans.*, 2013, **42**, 8498–8503.
63 D. H. Gibson, B. A. Sleadd and A. Vij, *J. Chem. Crystallogr.*, 1999, **29**, 619–622.
64 Y. Tamaki, T. Morimoto, K. Koike and O. Ishitani, *Proc. Natl. Acad. Sci. U. S. A.*, 2012, **109**, 15673–15678.
65 R. N. Sampaio, D. C. Grills, D. E. Polyansky, D. J. Szalda and E. Fujita, *J. Am. Chem. Soc.*, 2020, **142**, 2413–2428.
66 K. Ozawa, Y. Tamaki, K. Kamogawa, K. Koike and O. Ishitani, *J. Chem. Phys.*, 2020, **153**, 154302.
67 M. Takahashi, T. Asatani, T. Morimoto, Y. Kamakura, K. Fujii, M. Yashima, N. Hosokawa, Y. Tamaki and O. Ishitani, *Chem. Sci.*, 2023, **14**, 691–704.
68 P. Gotico, T. T. Tran, A. Baron, B. Vauzeilles, C. Lefumeux, M. H. Ha-Thi, T. Pino, Z. Halime, A. Quaranta, W. Leibl and A. Aukauloo, *ChemPhotoChem*, 2021, **5**, 654–664.
69 In this stage, the TON of CO production was 2–3. Based on the results shown in Fig. 5, only a small amount of **RuC2Re(CO-TEOA)** was produced. Therefore, the main reduced complex should be **(Ru)⁻C2Re(COOH)**.
70 Y. Tamaki, K. Koike, T. Morimoto and O. Ishitani, *J. Catal.*, 2013, **304**, 22–28.